Available online at www.sciencedirect.com
SCIENCE DIRECT®
International Journal of Heat and Fluid Flow 27 (2006) 154–166
International Journal of HEAT AND FLUID FLOW
www.elsevier.com/locate/ijhff

Numerical investigation of natural circulation in a 2D-annular closed-loop thermosyphon

Gilles Desrayaud [a,*], Alberto Fichera [b], Manuel Marcoux [a]

[a] INSSET/LETEM, Université de Picardie Jules Verne, 48 rue Raspail, BP 422, 02109 Saint-Quentin Cedex, France
[b] Dipartimento di Ingegneria Industriale e Meccanica, Università di Catania, Viale A. Doria 6, 95125 Catania, Italy

Received 9 December 2004; received in revised form 18 March 2005; accepted 7 April 2005
Available online 16 June 2005

Abstract

This work aims to investigate the natural convection in a water-filled closed-loop. A numerical study of laminar, two-dimensional natural convection in an annular thermosyphon is reported, the loop being heated at a constant flux over the bottom half and cooled at a constant temperature over the top half. The annular thermosyphon configuration which is the subject of this study has never been investigated previously. It is numerically demonstrated that the complexity of the dynamic properties encountered in the experimental studies of toroidal or rectangular loops, is found here: steady flow with and without recirculating regions, periodic motion and Lorenz-like chaotic flow. The numerical work also aims to simulate the variation of mass flow rate and heat transfer behaviors where the driving parameters and correlations which are non-loop specific are also given.

Keywords: Natural circulation loop; Annular thermosyphon; Thermal convection; Numerical research

1. Introduction

Natural circulation loops are systems in which the flow is driven by buoyancy forces created by heating and cooling of a fluid inside a closed or open pipe system placed in a vertical plane so that pumping is not required. Closed-loops have at least one heat source and one heat sink connected by pipes. The circulation is driven by buoyancy formed by a negative vertical temperature gradient, which yields reliability, and low-cost noise-free advantages. This device is a type of thermosyphon, a non-mechanical heat pump used for cooling purposes in industrial processes, including solar water heaters, geothermal processes, gas turbine blade cooling, and as part of the emergency core cooling system in nuclear reactors. Because of their practical importance, especially in energy plants in which safety is a stringent requirement, thermosyphons have been the subject of a large number of theoretical and experimental studies. A review of the wide applications of natural circulation loops in engineering systems has been given by Zvirin (1981). The research pioneered by Keller (1966), Welander (1967) and Malkus (1972) has also been reviewed by Greif (1988). The most common experimental loop geometries reported in the literature are the rectangular and the toroidal thermosyphons having uniform pipe diameter throughout the loop. The loops are often in some simple configuration such as circular toroidal loop heated uniformly over the lower half and cooled over the upper half through a constant wall temperature or an annular heat exchanger (Gorman et al., 1986; Stern et al., 1988; Jiang et al., 2002), or a rectangular thermosyphon loop with heating in the bottom part by a uniform heat flux source and cooling in the top part by a uniform-temperature heat sink (Huang and Zelaya,

* Corresponding author. Tel.: +33 3 23 62 89 59; fax: +33 3 23 62 89 35.
E-mail address: gilles.desrayaud@insset.u-picardie.fr (G. Desrayaud).

0142-727X/$ - see front matter © 2005 Elsevier Inc. All rights reserved.
doi:10.1016/j.ijheatfluidflow.2005.04.002

Nomenclature

a	gap width ($a = r_o^* - r_i^*$), m
c_p	specific heat of the fluid, J/(kg K)
f	stretched radial coordinate ($f = \eta r + 1$)
f_F	Fanning friction factor (Darcy–Weisbach friction factor $f_{DW} = 4f_F$)
g	acceleration due to gravity, m/s^2
Gr_m	modified Grashof number based on the hydraulic diameter, $2a$
Gz	Graetz number
$h(\theta)$	convective heat transfer coefficient, W/(m^2 K)
L	total length of the loop $\pi(r_i^* + r_o^*)$, m
Nu	Nusselt number
P	dimensionless pressure
Pr	Prandtl number ($Pr = \nu/\alpha$)
q	dimensionless total heat flux at the heater
q''	specific heat flux at the heater, W/m^2
Q	dimensionless mass flow rate
r	dimensionless radial coordinate ($\frac{r^* - r_i^*}{a}$)
r_i^*	inner cylinder radius, m
r_o^*	outer cylinder radius, m
R	radius ratio (r_o^*/r_i^*)
Ra	Rayleigh number ($Ra = g\beta a^3 \Delta T/\alpha\nu$)
Ra_{2a}	Rayleigh number based on the hydraulic diameter $2a$, $Ra_{2a} = 8Ra$
Re_{2a}	Reynolds number based on the hydraulic diameter $2a$
T	dimensional temperature, K
T_c	dimensional cold temperature, K
u, v	dimensionless radial and axial velocity
$\overline{V}$	dimensionless cross-sectionally average axial velocity
$\overline{V}^*$	dimensional cross-sectionally average axial velocity

Greeks

α	thermal diffusivity of the fluid, m^2/s
β	coefficient of thermal expansion of the fluid, K^{-1}
κ	thermal conductivity of the fluid, W/(mK)
ρ	fluid density, kg/m^3
μ	dynamic viscosity of the fluid, Ns/m^2
ν	kinematic viscosity of the fluid, m^2/s
η	curvature parameter $\eta = R - 1$
τ	dimensionless time ($\tau = \alpha t^*/a^2$)
θ	angular coordinate measured from downward vertical
Θ	dimensionless temperature ($\Theta = (T - T_c)/\Delta T$)
$\overline{\Theta}_b$	dimensionless bulk temperature
Θ_m	dimensionless mean temperature
ΔT	temperature difference ($\Delta T = aq''/\kappa$), K
ΔT_r	reference temperature difference, see Eq. (15), K
ΔZ	center line elevation difference between cooler and heater, m

Superscript

*	variable with dimension

Subscripts

c	cold exchanger
h	hot exchanger
i	inner cylinder
o	outer cylinder
w	at the walls (r_i^* and r_o^*)

1988; Bernier and Baliga, 1992; Vijayan and Austregesilo, 1994; Misale et al., 1998; Cammarata et al., 2002). Natural circulation loops also attract attention because of the variety of fluid motions and the complexity of the dynamic properties encountered, in spite of the simplicity of their geometry. The Lorenz-like chaotic alternations of flow direction were experimentally observed in toroidal thermosyphon by Creveling et al. (1975), Gorman et al. (1986), Ehrhard and Muller (1990) and in rectangular thermosyphon by Damerell and Schoenhals (1979), Vijayan and Austregesilo (1994), Misale et al. (1998), Cammarata et al. (2002) which was well described by the Lorenz model (Gorman et al., 1986; Ehrhard and Muller, 1990).

Most studies of closed-loops have utilized a one-dimensional approach by averaging the governing equations over the pipe cross-section, which required a priori specifications of the friction factor, loss coefficients and the heat transfer coefficients to be provided (as input). It is assumed that the velocity is solely in the axial direction and that the effects of the pipe curvature and axial conduction are negligible. Integrating the momentum equation around the loop reduces this equation to an overall balance between buoyancy and friction (Greif, 1988). It has been argued that the disagreement between analyses and experiments arises mainly from the adoption of the conventional forced flow friction factor correlation, 1D approximation and convection heat transfer correlations in the analysis.

Some attempts have been made to improve the 1D steady analysis. Mertol et al. (1982) were the first to propose a 1D/2D steady analysis of heat transfer and fluid flow in a toroidal thermosyphon. The flow is assumed to be in the axial, θ, direction only, i.e., radial and azimuthal velocities are neglected, while the temperature field is assumed to be in the radial and axial direction

(r and θ). Axial conduction, viscous dissipation, and the effects of curvature were neglected. A 1D/2D analysis was also carried out by Su and Chen (1995) for rectangular loop with horizontal and vertical heated sections, and satisfactory comparisons were performed with the results of Bernier and Baliga (1992). Misale et al. (2000) numerically extended the 1D/2D analysis to transient behavior of the loop and to the influence of wall thermal capacity of the pipe. Axial conduction both in the fluid and in the wall was also considered. Bernier and Baliga (1992) proposed a new model in which the governing equations were written in elliptic forms and the solving method involves an iterative procedure to couple the local results of 2D numerical simulation performed in the heated and cooled sections with those of the 1D analysis performed in other sections of the thermosyphon. Recently, Basaran and Kucuka (2003) studied a rectangular thermosyphon using an experimental set-up and numerical technique similar to that of Bernier and Baliga (1992). Their model provides meaningful results with the experiments for calculating heat transfer rate, while discrepancy arises at the highest values of the Grashof number. In addition velocity and temperature profiles in the heated and cooled sections can be obtained.

Conventional forced flow correlations for fully developed flow are assumed to be applicable to natural circulation flow in 1D analyses. In a closed-loop, however, due to flow area changes, the presence of bonds, etc. the flows are often not fully developed. It seems that the overall loss coefficient under forced flow conditions, K (friction factor + local loss coefficients), fails to predict the natural circulation data because of the failure to account for the effect of secondary flows under natural circulation conditions that become particularly important at large Ra numbers. Several past proposals for correlating the overall hydraulic loss coefficient are reviewed and a generalized correlation was proposed that is non-loop specific (Vijayan et al., 1991). Vijayan and Austregesilo (1994) also developed scaling laws for natural circulation loops for steady state flows and stability analysis which are non-loop specific. They successfully tested correlation against experimental data from various loops. This non-dimensionalization procedure was recently extended to non-uniform diameter loops by Vijayan (2002). These simple non-dimensional groups can easily be calculated from the known geometry and the operating conditions of the loop.

To our knowledge, no direct unsteady 2D numerical simulations exist in the literature and only one numerical experiment on steady 3D flow in a toroidal loop can be found (Lavine et al., 1987). The purpose of the present study is to investigate by direct numerical integration of the governing equations, the steady and unsteady motions in a thermosyphon of simple well-defined geometry, a 2D-annular loop. The influence of the Rayleigh number on the performance of the loop has been studied by running five series of simulations. The numerical results have been analyzed to find the principal dimensionless parameters and the correlations between the Reynolds number, frictional factor and Nusselt number.

2. Analysis and numerical resolution

2.1. Governing equations

Consider an annular loop of laminar incompressible fluid heated over one-half its area at a uniform heat flux (q'') and cooled over the upper half through a constant wall temperature (T_c) as shown in Fig. 1. For the numerical analysis of the annular thermosyphon, the flow is assumed two-dimensional and natural convection is considered in a plane perpendicular to the axis of the annulus. The cylindrical coordinate system is defined so that the r^*-axis is in the radial direction with the origin at the axis of the annulus and θ is the angular coordinate measured from the downward vertical in the anti-clockwise direction. The inner (respectively outer) cylinder radius is r_i^* (resp., r_o^*), the channel gap being defined as, $a = r_o^* - r_i^*$. The classical governing equations (Navier–Stokes plus energy) for unsteady incompressible flows of a Newtonian fluid with the Boussinesq approximation used in cylindrical coordinates, may be written in dimensionless form as

$$\frac{\partial}{\partial r}(fu) + \eta\frac{\partial v}{\partial \theta} = 0 \tag{1}$$

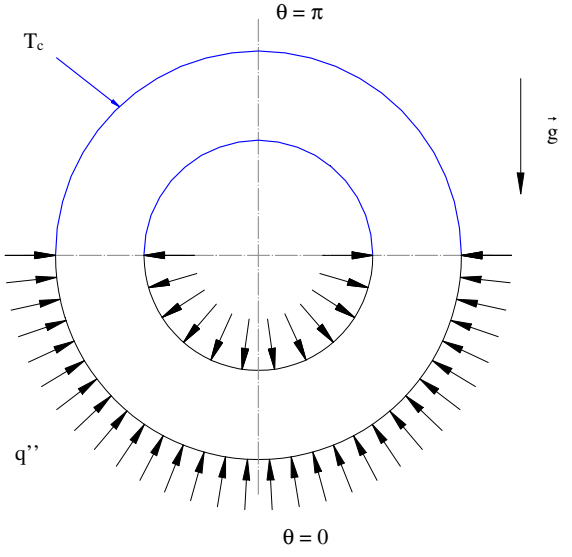

Fig. 1. Coordinate system and geometry.

$$\frac{\partial}{\partial\tau}(fu)+\frac{\partial}{\partial r}(fuu)+\frac{\partial}{\partial\theta}(\eta vu)-\eta v^2 = -f\frac{\partial P}{\partial r}-Ra\,Prf\Theta\cos\theta + Pr\left(\frac{\partial}{\partial r}\left[f\frac{\partial u}{\partial r}\right]+\frac{\partial}{\partial\theta}\left[\frac{\eta^2}{f}\frac{\partial u}{\partial\theta}\right]-\frac{2\eta^2}{f}\frac{\partial v}{\partial\theta}-\frac{\eta^2}{f}u\right) \quad (2)$$

$$\frac{\partial}{\partial\tau}(fv)+\frac{\partial}{\partial r}(fuv)+\frac{\partial}{\partial\theta}(\eta vv)+\eta uv = -f\frac{\partial P}{\partial\theta}+Ra\,Prf\Theta\sin\theta + Pr\left(\frac{\partial}{\partial r}\left[f\frac{\partial v}{\partial r}\right]+\frac{\partial}{\partial\theta}\left[\frac{\eta^2}{f}\frac{\partial v}{\partial\theta}\right]+\frac{2\eta^2}{f}\frac{\partial u}{\partial\theta}-\frac{\eta^2}{f}v\right) \quad (3)$$

$$\frac{\partial}{\partial\tau}(f\Theta)+\frac{\partial}{\partial r}(fu\Theta)+\frac{\partial}{\partial\theta}(\eta v\Theta) = \frac{\partial}{\partial r}\left[f\frac{\partial\Theta}{\partial r}\right]+\frac{\partial}{\partial\theta}\left[\frac{\eta^2}{f}\frac{\partial\Theta}{\partial\theta}\right] \quad (4)$$

with $\eta = R - 1$ and $f = f(r) = \eta r + 1$, R being the radius ratio.

The numerical code employed in the present investigation has been used in Cadiou et al. (1998) and Desrayaud et al. (2000) and has been shown to be accurate and reliable for unsteady flows at low Prandtl number. The way in which the equations are non-dimensionalized is different from that of the cited papers, and the governing equations are here put into dimensionless forms by scaling length, time, velocity and temperature as

$$r=\frac{r^*-r_i^*}{a};\quad \tau=\frac{\alpha t^*}{a^2};\quad u=\frac{au^*}{\alpha};\quad v=\frac{av^*}{\alpha};$$
$$\Theta=\frac{T-T_c}{\Delta T}\ \text{with}\ \Delta T=\frac{aq''}{\kappa}$$

The dimensionless boundary conditions are the following:

Heating section $-\pi/2\leqslant\theta\leqslant\pi/2$,

$$r=0\ \text{and}\ 1\quad u=v=0\quad \frac{\partial\Theta}{\partial r}=-1 \quad (5)$$

Cooling section $\pi/2\leqslant\theta\leqslant 3\pi/2$,

$$r=0\ \text{and}\ 1\quad u=v=0\quad \Theta=0$$

2π-periodicity in the θ direction $0<r<1$,

$$u,v,P,\Theta|_{\theta=0}\quad =u,v,P,\Theta|_{\theta=2\pi} \quad (6)$$

The motionless and isothermal solution used as the initial guess for computations is given by

For $\tau=0$ at $0<r<1$ and $0\leqslant\theta\leqslant 2\pi$,

$$u=v=0\quad \Theta=0 \quad (7)$$

The non-dimensional parameters that govern the flow are the Rayleigh number Ra, the Prandtl number Pr and the radius ratio R which are defined by

$$Ra=g\beta a^3\Delta T/\alpha\nu(=Ra_{2a}/8)\quad Pr=\nu/\alpha\quad R=r_o/r_i \quad (8)$$

2.2. Non-dimensional numbers

The local Fanning friction factor f_F on the inner and outer walls is calculated as

$$f_F=-\frac{\mu r^*\frac{\partial}{\partial r^*}\left(\frac{v^*}{r^*}\right)\Big|_w}{\frac{1}{2}\rho\overline{V}^{*2}}=-\frac{2fPr}{\overline{V}^2}\frac{\partial}{\partial r}\left(\frac{v}{f}\right)\Big|_w \quad (9)$$

where $\overline{V}=\int_0^1 v\,dr$ is the non-dimensional cross-sectional average velocity. This is the same thing as the dimensionless mass flow rate, Q. The Darcy–Weisbach friction factor is related to the Fanning friction factor by $f_{DW}=4f_F$.

For forced laminar flow in a planewall channel, thus neglecting the curvature effect, the Fanning friction factor can be analytically calculated and is equal to $24/Re_{2a}$. The Reynolds number Re_{2a}, based on the hydraulic diameter $2a$, is equal to $Re_{2a}=\frac{\rho\overline{V}^*2a}{\mu}$.

The local Nusselt numbers at the heater and at the cooler are evaluated for each wall as

$$Nu_h(\theta)=\frac{h(\theta)2a}{\kappa}=\frac{2}{\Theta_w-\Theta_b}\quad Nu_c(\theta)=\frac{2}{\Theta_b}\frac{\partial\Theta}{\partial r}\Big|_w \quad (10)$$

Θ_w is the wall temperature and Θ_b the bulk temperature,

$$\Theta_b(\theta)=\frac{\int_0^1 v\Theta\,dr}{\overline{V}} \quad (11a)$$

The following non-dimensional parameters also need to be defined:

$$\text{the mean temperature}\ \Theta_m(\theta)=\int_0^1\Theta\,dr \quad (11b)$$

and the total heat flux at the heater through the inner and through the outer walls:

$$\bar{q}_i=\frac{\pi}{R-1}\quad\text{and}\quad\bar{q}_o=\frac{\pi R}{R-1} \quad (11c)$$

The mean values of the Nusselt number at the walls of the annulus are calculated as

$$\overline{Nu}_{\text{inner/outer}}=\frac{1}{\pi}\int_{\theta_0}^{\theta_0+\pi}Nu(\theta)d\theta,$$

$\theta_0=-\pi/2$ at the heater and $\pi/2$ at the cooler. (12)

and the mean values on halves the annulus (heater and cooler) are thus equal to:

$$\overline{Nu}_{h/c}=\frac{\overline{Nu}_{inner}+R\overline{Nu}_{outer}}{1+R} \quad (13)$$

As can be seen in the next paragraph, the Nusselt numbers are not well suited to the present problem (because the denominator of Nu_h can be zero) but are given here for the sake of comparison with previous papers.

2.3. Numerical resolution

The control volume procedure is utilized to discretize on a staggered, uniform cylindrical grid the non-linear

system of governing equations and boundary conditions with the second order centered scheme for the convective terms. The SIMPLER algorithm is employed to solve the coupling between continuity and momentum equations through pressure. All the conservation equations were cast in transient form with a semi-implicit scheme for temporal integration, the Alternating Direction Implicit (ADI) method. Boundary conditions of periodic type were applied at $\theta = 0$ and 2π. This consists of using the solutions calculated at a previous radial sweeping as the boundary conditions in the angular sweeping of the ADI procedure.

Firstly, to check the adequacy of the numerical scheme employed for solving the full elliptic governing equations, the computational code was validated on several cases, close to this particular problem, for which experimental or numerical data are available. These cases are chosen so as to verify that the code was properly implemented. These are

- steady motion in a differentially heated annulus of large radius ratio $R = 2.6$ (Kuehn and Goldstein, 1976); a thermal steady plume occurs on the top part of the annulus;
- periodic motion in a differentially heated annulus of small radius ratios $1.04 \leqslant R \leqslant 1.24$. A time-dependent convective pattern of Rayleigh–Bénard-like rolls occurs on the top part of the annulus (Powe et al., 1969). Hydrodynamic instabilities located within the crescent main flow at the vertical portions of the annulus also exist (Cadiou et al., 1998).

Satisfactory agreement was obtained in both cases.

In Table 1, the mean Nusselt number is compared with the numerical values found by Kuehn and Goldstein (1976), for steady flows in a differentially heated annulus. The values of the mean Nusselt number obtained on the same grids using a finite element code (TRIO-EF developed at the French Atomic Energy Center in Saclay) are also given (Cadiou, 1997). As shown, a quite good agreement was found with a maximum relative error of 5% for Rayleigh numbers lower than 10^3 and a relative error better than 1% for $Ra \geqslant 10^4$. While using the same computational code as Cadiou, our results are slightly different because we used a finer grid (30×240 instead of 41×120). Had we used the same grid as Cadiou, we would obviously have obtained the same results. One can also refer to papers of Cadiou et al. (1998) and Desrayaud et al. (2000) for validation of the computational code for unsteady motions in the case of small radius ratios, their code being used in the present study.

Table 1
Comparison of the mean Nusselt numbers for a differentially heated annulus, $R = 2.60$ and $Pr = 0.7$

Ra	Cadiou (1997) (41, 120) FV	Cadiou (1997) FE	Kuehn and Goldstein (1976)	Present results (30, 240)
10^3	1.085	1.075	1.081	1.109
10^4	1.987	1.957	2.010	2.004
5×10^4	2.944	2.891	3.036	3.031

FV: Finite volume. FE: Finite element.

Table 2
Mean and local values for various grid systems, $Ra = 12\,500$, $R = 2.0$, $Pr = 5$

(N_r, N_θ)	Re_{2a}	$f_F Re_{2a}$	$\overline{Nu}_c$	$\overline{Nu}_h$	$\overline{\Theta}_h$	$\overline{\Theta}_b$	$\Theta_{0,in}$	$\Theta_{0,out}$
(20, 184)	12.73	23.56	9.106	17.03	0.4800	0.2455	0.4245	0.5179
(20, 320)	12.58	23.38	9.084	31.14	0.4836	0.2460	0.4292	0.5190
(30, 320)	12.60	23.91	9.094	11.65	0.4821	0.2454	0.4265	0.5276
(40, 320)	12.44	24.19	9.083	11.35	0.4822	0.2449	0.4283	0.5326
(40, 360)	12.60	24.14	9.094	21.38	0.4821	0.2449	0.4265	0.5320

Secondly, grid refinement studies were conducted for several radius ratios to ensure accuracy. Some results are reported in Table 2 for a closed-loop of radius ratio $R = 2.0$. The number of points in the radial and angular directions is denoted N_r and N_θ. To determine the appropriate grid size for obtaining grid-independent solutions, the computations were done on increasingly finer grid size distributions. The parameters used to check the grid independence of the computational results were local and average values of various variables and are given in Table 2 for various grid arrangements. It is noted that the differences in the mean and local values between the (30, 320) and the (40, 360) grids are all less than 1% except for the Reynolds number for which the difference reaches 1.2%. Attention must be paid to the mean Nusselt number at the heater, whose values appear to be non-coherent. This is not due to numerical error but to the definition (see Eq. (10)) in which temperature difference appears as the denominator. Looking at the mean and wall temperature evolutions along the loop (not shown here), it can be seen that there is cross-over between the curves at the exit of the heat exchanger leading to very high positive or negative values of the local Nu and thus to these incoherent values of the mean Nusselt number at the heater (Table 2). This is why in the following the mean temperature at the heater is used instead of the mean Nusselt number.

The result of this grid refinement study was to select uniform meshes having at least 30×320 control volumes in the r and θ directions for steady flows and for possibly oscillating and reverse flows. This grid system was considered as a good compromise between the accuracy of the solutions and CPU-time. All the finite volume calculations were carried out on a NEC-SX5 with a 1 Gflop-speed on average.

3. Results and discussion

The behavior of a natural circulation loop has been investigated numerically. The transient and steady-state

results will be presented first on a typical solution at radius ratio, $R = 2$ which is discussed in depth, the same behavior occurring for all the other radius ratios studied, $R = 1.8$, 1.6, 1.4, 1.2 and 1.08. The working fluid in the thermosyphon was water with Prandtl number, $Pr = 5$ in all cases.

Upon increasing the Rayleigh number, several steady-state and time-dependent flow patterns develop, as was experimentally observed by Creveling et al. (1975) in toroidal loop: pure conduction (no flow); steady circulation in either the clockwise or counter-clockwise direction; neutrally stable oscillations in which the flow oscillated about the mean flow as it circulated around the loop (this regime occurred for only one value of the transfer at the heat exchanger); and unstable oscillations in which the fluid oscillated about the mean flow with increasing amplitude until the mean flow direction reverses.

3.1. Steady flow

Due to the symmetry of the heating and cooling sections to the vertical axis, the flow can be clockwise or counter clockwise by chance. At very low values of the Rayleigh number (Fig. 2a), the global motion all around the loop is almost inexistent and two very large recirculations of weak motion occur. The stratified temperature distribution in Fig. 2b reveals the importance of the axial conduction.

The Reynolds number Re_{2a} is equal to 0.015 when $Ra = 10$ and $R = 2.0$, which means that the heat transfer by convection is much lower than the heat diffusion and in practice, the global convection in the loop is not easily distinguishable. Fig. 2c shows angular temperature profiles along the inner and outer walls of the hot exchanger and also in the middle of the gap. The fairly good superposition of the temperature profiles of both halves ($[-\pi, 0]$ and $[0, \pi]$) of the hot exchanger is evidence that convection plays only a minor role in the heat transfer and that the heat is mainly transferred by conduction from the lower hot part to the upper cold part, the temperature profiles being almost linear in the "vertical" legs ($[-\pi, -\pi/2]$ and $[\pi/2, \pi]$).

This regime was qualified by Gorman et al. (1986) as absolutely stable because it corresponds to a fixed point in the 3D state space whose axes are the fluid velocity, the temperature at six o'clock (0 radian) and the temperature difference between nine o'clock ($-\pi/2$ radian) and six o'clock $T_9 - T_6$. A steady temperature field was maintained in the fluid and they concluded that the fluid motion is non-existent. As Gorman et al. detected circulation by measuring the temperature difference $T_9 - T_6$, the temperature field of Fig. 2b which is symmetric by the vertical plane explains well why they failed to detect any global motion. The motion is so weak that one can consider that axial conduction prevails and it can be appropriately qualified as pseudo-conduction regime. It should be noticed that Jiang et al. (2002) did not find fluid at rest at the smallest heating power in their experiment with a toroidal loop made with copper pipe. Instead, the flow was steady.

In Fig. 3, the squared Reynolds numbers are plotted against the Rayleigh number for various values of the radius ratio. This Figure shows that these values can be accurately fitted by different but single straight lines for each radius ratio with the same critical value of the Rayleigh number (onset of the convective motion) very close to zero, in fact inside the gap [−4, 4]. Best fits give accurate results up to $Ra = 1.25 \times 10^4$, the power law being followed far beyond the threshold of convective motion. This is a well-known behavior as remarked by Sano (1991).

The temperature field is shown to change with Ra (see Figs. 2b, 5b, and 6b). With an increase in Ra, the isotherm contours begin to deflect suggesting the development and intensification of convection. A quasi-one-dimensional flow thus exists along the loop for moderate values of the Rayleigh number and the flow is steady without undergoing any oscillatory process. With increase in Ra, the fluid flow undergoes a short time-oscillation before becoming stable (Fig. 4a). The stream function, temperature and axial velocity fields for $Ra = 12\,000$ and $R = 2$ are shown in Fig. 5, the fluid

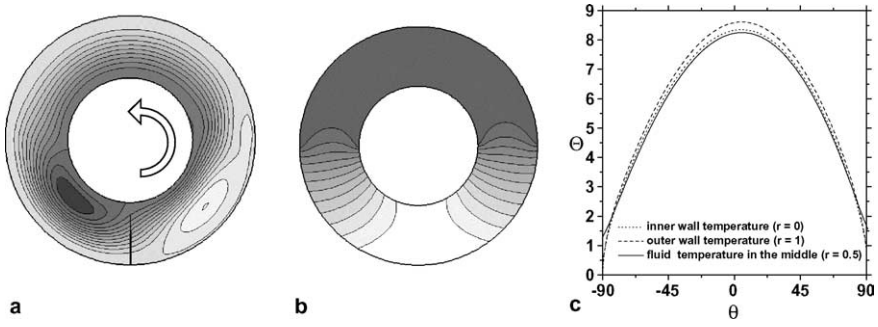

Fig. 2. Pseudo-conductive regime, $Ra = 10$, $R = 2$, $Pr = 5$: (a) stream function; (b) isotherms; (c) angular temperature profiles.

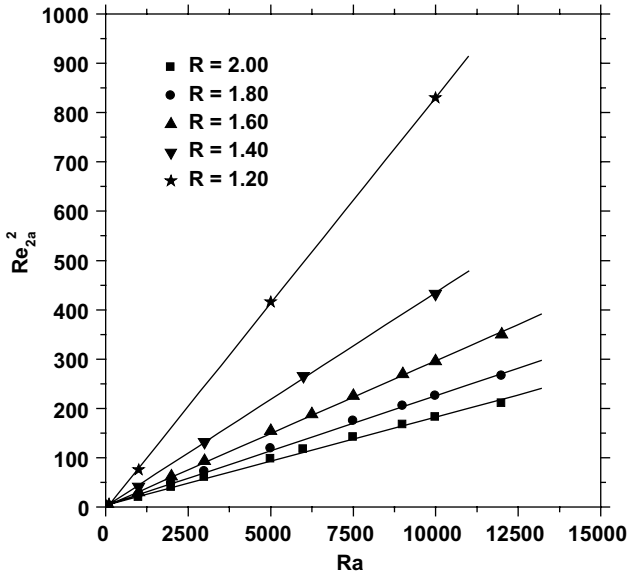

Fig. 3. Evolution of the square of *Re* as a function of the Rayleigh number for various radius ratios.

moving around the loop in a counter-clockwise direction. A zone of very strong temperature increase is clearly visible at the entrance of the heater along the outer wall (Fig. 5b, arrow (1)). On the other hand, this phenomenon does not exist at the cooler entrance due to the imposed temperature at the walls (Fig. 5b, arrow (2)). The streamlines that were concentric for low values of the Rayleigh number are now slightly deformed at the entrance of the exchangers, the streamlines being more distorted at the heater (Fig. 5a). This prefigures what follows. Fig. 4b shows the temporal evolution of the mass flow rate during the transient process from $Ra = 10\,000$ to $Ra = 12\,500$. The occurrence of the cells at the exchanger entrances is responsible for the decrease in the global mass flow rate inside the loop which is clearly visible in Fig. 4b. It should be emphasized here that the transient processes discussed above eventually approach stable flow. This is due to the fact that, for all the given operating conditions, the disturbances will be damped out and such a stable and steady flow will eventually occur. At $Ra = 12\,500$ (Fig. 6), it should be noted that, in addition to the circulatory main flow, two cells in the second and in the fourth quadrant can be seen. These two recirculating regions occur near the outer wall of the entrance of the heat exchangers (Fig. 6a and c). As a consequence, the zone of the strong temperature increase that extended largely downstream along the outer walls is now reduced (Fig. 6b, arrow (1)). The reverse flow is larger in the heating section than in the cooling section. This is because a constant wall-heat flux boundary condition allows greater temperature variation along the wall than does a constant wall-tem-

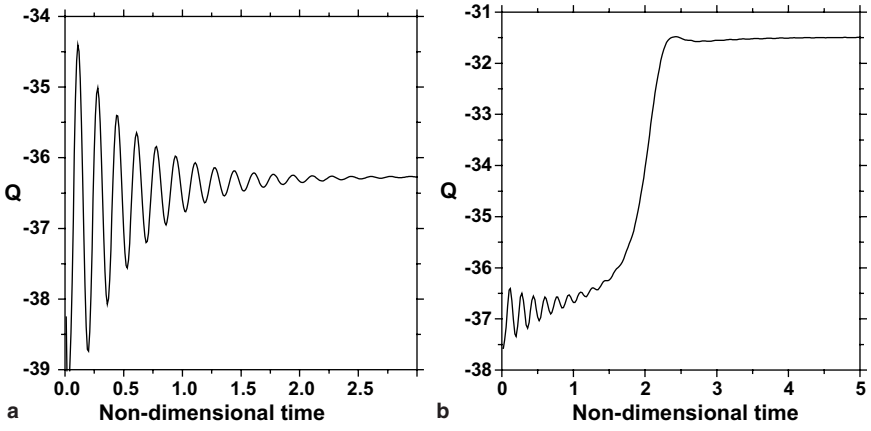

Fig. 4. Temporal evolution of the mass flow rate (Q) during transient state (initial state: $Ra = 10\,000$): (a) $Ra = 12\,000$ and (b) $Ra = 12\,500$.

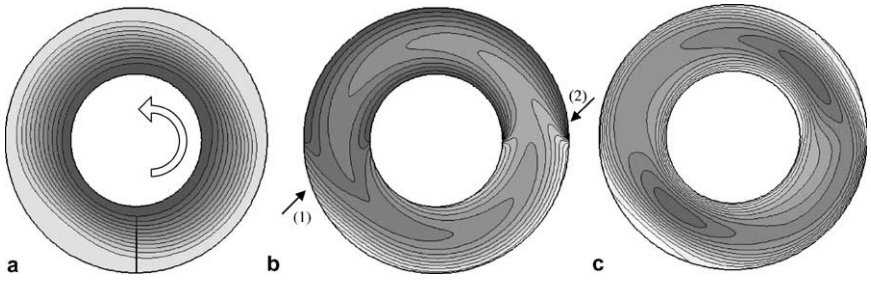

Fig. 5. Steady motion, $Ra = 12\,000$, $R = 2.00$, $Pr = 5$: (a) stream function; (b) isotherms; (c) axial velocity field.

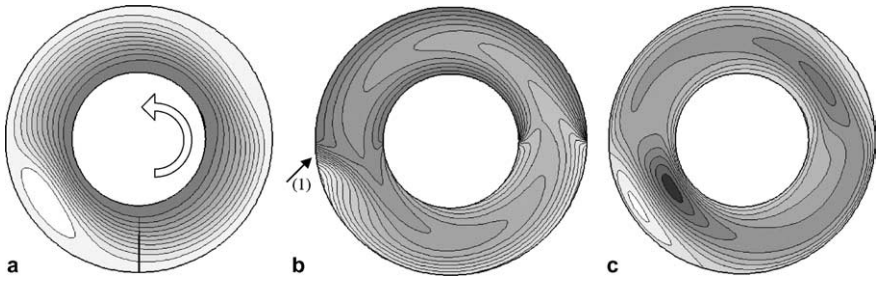

Fig. 6. Steady motion, $Ra = 12\,500$, $R = 2$: (a) stream function; (b) isotherms; (c) axial velocity field.

perature boundary condition. These cellular structures appear at values of the Rayleigh number close to 13 000 which also represents the upper limit of the steady motion.

The dimensionless temperatures profiles at the inner and outer wall are shown in Fig. 7a and b only along the heater, the cooler being at an imposed temperature. The temperature of the outer wall is always largely greater than the temperature of the inner wall. This is due to the boundary condition, imposed heat flux at the heater, combined with the curvature. Since the surface of the outer wall is R times greater than the surface of the inner wall, the total heat flux (Eq. (11c)) transferred to the convective fluid flow is also R times greater and there results a higher level of temperature at the outer wall. At $Ra = 10\,000$, the average temperature of the outer wall is $\bar{\Theta}_{h,outer} = 0.535$ while it is only 0.387 at the inner wall. At the entrance of the heater (first half-quarter), the outer wall temperature increases sharply (Fig. 7a, $Ra = 5000$, 10 000, 12 000). After that, the slope of the temperature profiles become smoother ($Ra = 5000$) in the remainder of the heater with a very abrupt decrease at the exit of the heater. When the Rayleigh number is increased to 10 000, a plateau with an almost constant temperature occurs (Fig. 7a, $Ra = 10\,000$). Close to the onset of the occurrence of the

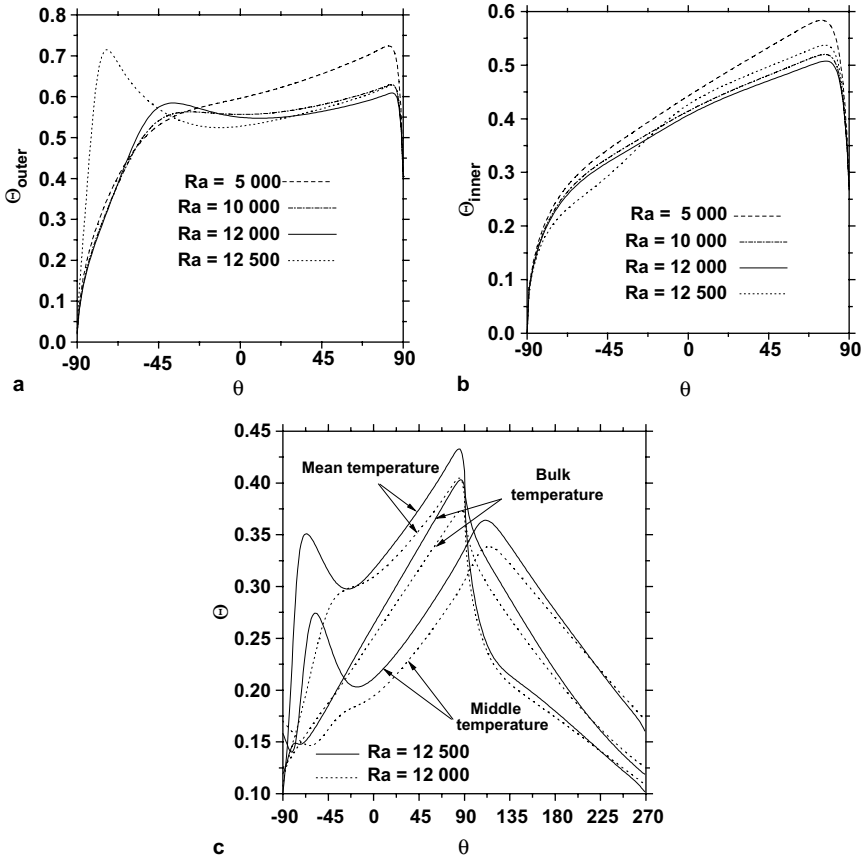

Fig. 7. Temperature along the loop for various Rayleigh numbers (a) outer wall; (b) inner wall; (c) bulk and mean temperatures.

recirculating flow ($Ra = 12\,000$), an inverse temperature gradient occurs just after the sharp increase of the outer wall temperature. This can, for a sufficiently strong inverse temperature gradient, create recirculating flow along the outer wall and give rise to a vortex which amplifies the inverse temperature gradient (Fig. 7a, $Ra = 12\,500$). Fig. 7c, giving the mean, bulk temperatures and temperature in the middle of the channel, shows that the flow entering the heater is strongly heated in the first half-quarter of the heat exchanger. The slight decrease in the outer wall temperature causes a slowing down of the fluid near the wall and recirculating flow for sufficiently high values of the Rayleigh numbers. This creates conditions for the occurrence of recirculating flow, and a temperature peak can be seen with a sharp decrease in the temperature at the heater entrance (Fig. 7a and c, $Ra = 12\,500$). The temperature peak does not exist for the bulk temperature, Θ_b, due to its definition, which is a velocity-weighted average temperature (Eq. (11a)). On the other hand, this peak exists for the mean temperature Θ_m (Eq. (11b)), which is just an area-weighted temperature. This difference reflects the irregularity of the axial velocity spatial distribution. The local temperature in the middle of the channel is largely lower than the mean temperature over the gap in the heat exchanger while in the cold exchanger the temperature in the middle of the channel is largely higher than the mean temperature. This is mainly due to the wall temperature being higher (respectively lower) than the temperature in the middle of the gap loop in the heater (resp. cooler).

The temperature and velocity fields of the flow in 2D-annular thermosyphons mainly differ in two ways from those in toroidal loop. Firstly, the local flow recirculation only exists in the neighborhood of the connections, although it wholly prevails in toroidal loops (Lavine et al., 1987). Secondly, these recirculations are along the outer cylinder. This is due to the fact that the two cylinders of the annulus are disconnected in 2D-analysis (or assumed to be connected far from the central vertical plan of the annulus if it is long enough). Consequently there is no heat transferred from one wall to another by conduction. Moreover in the present case, there is obviously no cross-stream secondary motion (i.e., motion perpendicular to the axial or θ direction).

3.2. Periodically oscillatory flow

Some authors have shown analytically and confirmed experimentally that steady flow is not achievable in a closed-loop thermosyphon for a certain range of heat inputs. In the present study, for Rayleigh numbers greater than 13 800, the flow first begins to oscillate periodically with a constant amplitude of very small magnitude. This is shown in Fig. 8 ($Ra = 13\,830$) which presents the time variation of the mass flow rate Q during some periods. The whole of the fluid in the loop oscillates weakly en bloc, not only with the same amplitude whatever the position (into the heater or into the cooler) but also with the same phase. During the periodic motion, the two cells oscillate on the spot, their strength (and size) varying slightly. In the phase space associated with the time variation of the mass flow rate (Fig. 8), the limit cycle (not shown here) clearly indicates that the motion is periodic with one frequency, $f = 5.76 \pm 0.10$. Temperature and velocities at various locations in the loop show identical values of the frequency. It should be remarked that this kind of periodically oscillatory flow is extremely difficult to stabilize: either the amplitude of the oscillations is slowly damped out ($Ra = 13\,800$) or it increases continuously ($Ra = 13\,850$), leading after a very long time to reverse flow (as we can assume). For $R = 2.00$, we only succeeded in obtaining one value (or a very small gap width) of the Rayleigh number at which it seems that the periodicity is guaranteed, i.e., $Ra = 13\,830$. This was also experimentally observed by Creveling et al. (1975) for the toroidal loop.

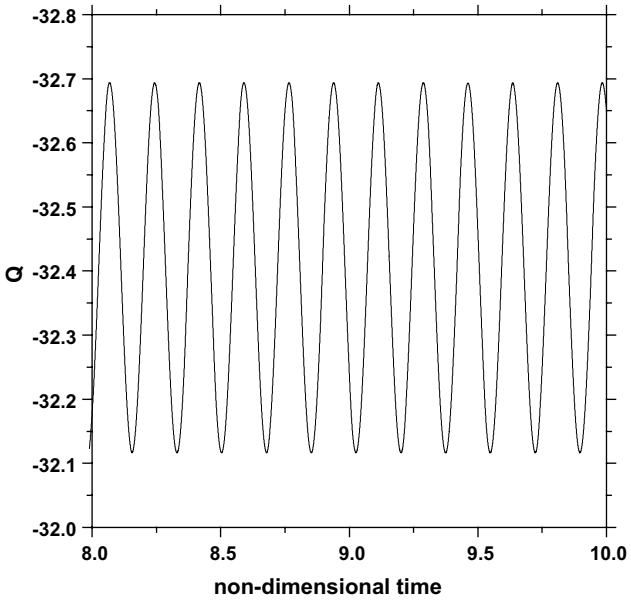

Fig. 8. Time history of the mass flow rate (Q), $Ra = 13\,830$, $R = 2$.

3.3. Reverse flow and Lorenz-like chaotic flow

For Rayleigh numbers greater than 15 000, unstable flow occurs and the flow rate oscillates with increasing amplitude until it eventually reverses direction, whereupon oscillations initiate in a new flow direction. Fig. 9a presents the time history of the mass flow rate Q at the middle of the cooler $(0.5, \pi)$. This variable clearly indicates the changes of flow direction with its change of sign. The oscillations would build up and the flow would again reverse after a (random) number of oscillations. Compared to Fig. 6, the positions of the two cells

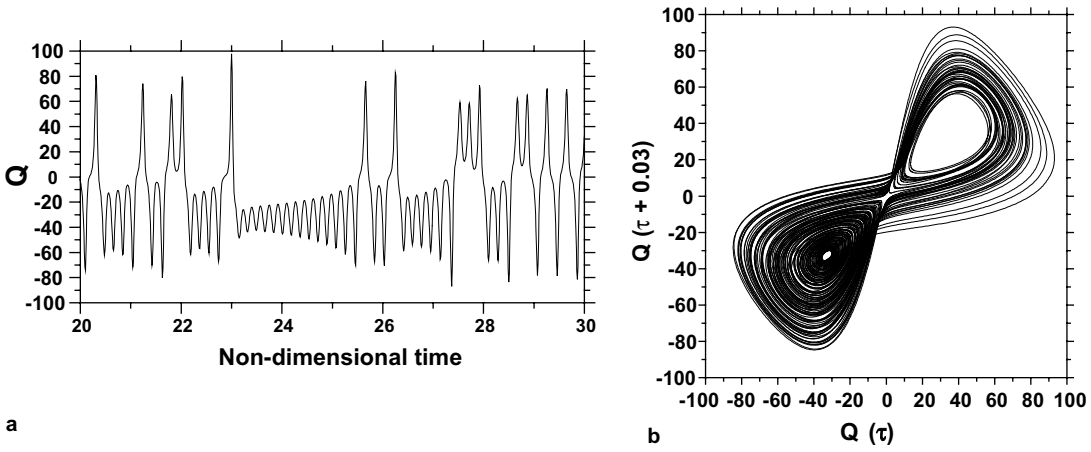

Fig. 9. Reverse flow and Lorenz-like attractor, $Ra = 15000$, $R = 2$: (a) time history and (b) Lorenz attractor.

are irregularly shifted to the first and third quadrant of the loop. Several experiments on the thermal convection in a closed-loop have been made and some of their results show Lorenz-like behavior (Creveling et al., 1975; Cammarata et al., 2002) as in the present numerical experiment, Fig. 9b showing the recognizable shape of the Lorenz attractor. This phase portrait has been built with only one time series (horizontal axis), that of the mass flow rate given in Fig. 9a and using a time step lag of 0.03 for the other one (vertical axis).

3.4. Heat transfer results

Fig. 10 shows the local Nusselt number (Eq. (10)) along the loop for various values of the Rayleigh number. As explained before, oscillations can be found at the heater exit but are not given here for clarity. It can be seen that the Nusselt number is almost insensitive to the increase of the Rayleigh except at $Ra = 12500$ for which a recirculation exists at the heater entrance. Two values are also shown in Fig. 10 (symbolized by two horizontal full lines) which are the asymptotic values for fully developed laminar flow inside a plane wall channel for uniform heating (8.235) and for constant wall temperature (7.54), respectively. The local Nusselt numbers are far from these asymptotic values, especially those at the heater, even at low Rayleigh number. This is in clear contradiction to what was predicted by 1D/2D analysis.

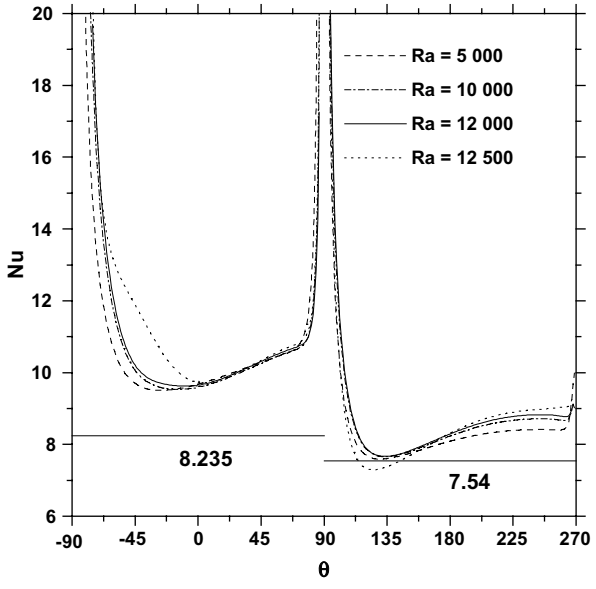

Fig. 10. Local Nusselt number for various Rayleigh numbers, $R = 2$.

A Graetz-like number was introduced as a parameter by Mertol et al. (1982) in their 1D/2D analysis of natural convection loops and variations of friction factor, and heat transfer coefficients along the loop were given versus this non-dimensional number. This number is equal to:

$$Gz = Re_{ch} Pr \left(\frac{2a}{L}\right) \quad \text{with} \quad Re_{ch} = \frac{\rho V^*_{ch}(2a)}{\mu} \quad \text{and}$$

$$V^*_{ch} = \left[\frac{g\beta a q''}{2\pi\mu c_p}\left(\frac{r^*_i + r^*_o}{2}\right)\right]^{0.5} \tag{14}$$

The dimensionless characteristic velocity V^*_{ch} used to build the characteristic Reynolds number Re_{ch} is derived based on an overall balance between buoyancy and friction as was done for the first time by Creveling et al. (1975) in a one-dimensional analysis. In the present work, the same characteristic velocity is used (see Eq. (14)) because the same kind of formula is found to within one constant. It follows that the Graetz-like number is proportional to $[Ra_{2a}(R-1)/(R+1)]^{0.5}$.

The mean Nusselt number at the cooler (Eq. (13)) is presented in Fig. 11 for various radius ratios. It is found that the best presentation of the variation of the mean Nusselt number at the cooler is with the non-dimensional number, $[Ra_{2a}(R-1)/(R+1)]^{0.5}$. It is then shown that the mean Nusselt number levels out to an

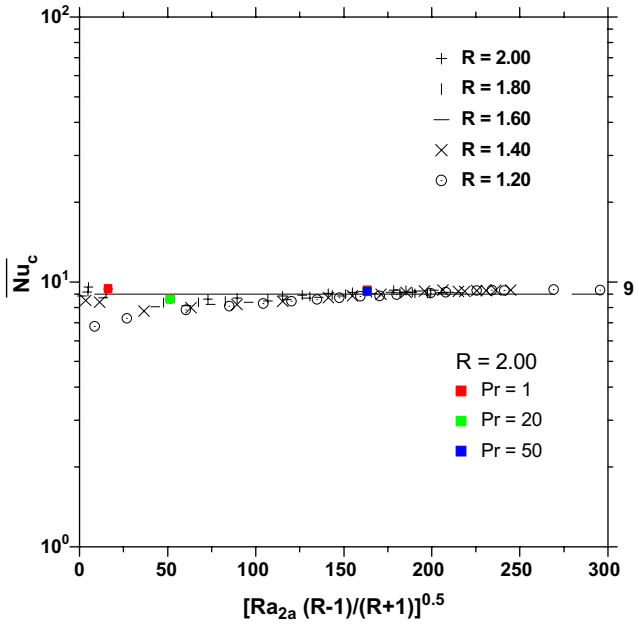

Fig. 11. Mean Nusselt number at the cooler for various radius ratios.

asymptotic value close to 9. This value is higher than the asymptotic value for fully developed laminar flow inside a plane wall channel for constant wall temperature (7.54). As explained before, instead of presenting the Nusselt number at the heater, wall heater mean temperature is given in Fig. 12 versus the same non-dimensional number $[Ra_{2a}(R-1)/(R+1)]^{0.5}$. All the wall mean values follow the same trend independently of the radius ratios and converge, for the highest values,

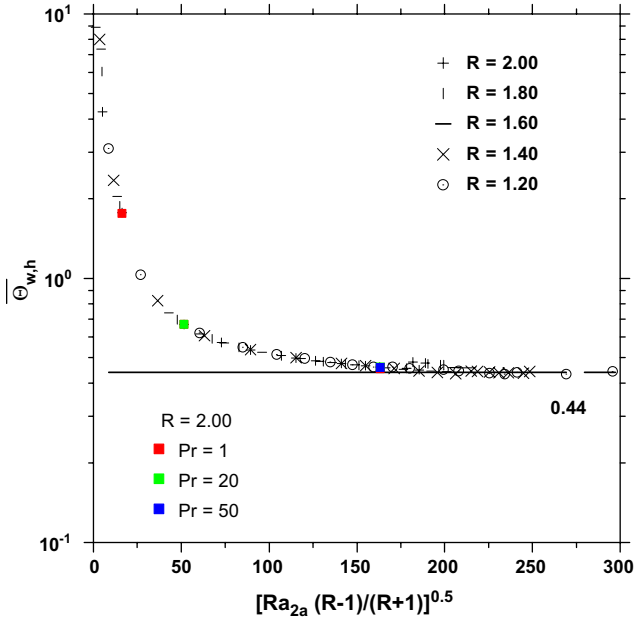

Fig. 12. Wall heater mean temperature for various radius ratios.

to the 0.44 value. This shows that this non-dimensional number is well designed to present heat transfer parameters as mean Nusselt numbers or mean temperatures.

3.5. Generalized Reynolds number correlation

For several decades, correlations proposed to link dynamical and heat transfer coefficients to driving parameters, under steady state natural circulation conditions, have always used either dimensional or loop-specific non-dimensional groups. It appears that one of the limitations of the 1D analytical studies, and thus of the deduced correlations, was the use as input of an unsuitable formula for the friction factor and heat transfer coefficients, established for fully developed forced flow and not for the specific case of natural circulation loops.

Recently, Vijayan and Austregesilo (1994) demonstrated, that for the steady state behavior of natural circulation loop, it is only necessary to simulate a single non-dimensional parameter which is non-loop specific, namely, $Gr_m(D_h/L)$. They carried out experiments in three rectangular, natural circulation loops of different pipe diameters. They succeeded in developing scaling laws for single-phase natural circulation loops based on these experiments, and using a simple 1D analysis as did Zvirin (1981). This non-dimensionalization procedure was extended by Vijayan (2002) to non-uniform diameter loops, as most practical applications employ loops of non-uniform diameter.

Surprisingly, the comparison of their generalized correlation against data of uniform and non-uniform diameter loops showed that secondary flows and the undeveloped nature of the flow are of small importance vis-à-vis accounting for local pressure losses. Moreover, in the calculation of the overall loss coefficient, they used the conventional forced flow correlation for friction factor and took into account the loss coefficients if they were significant. The generalized correlation is in good agreement with the experimental data of Huang and Zelaya (1988) who were the only ones to account for the local pressure losses. Vijayan (2002) claimed that the observed deviations from the theoretical correlation can be attributed mainly to the unaccounted local pressure losses in loops which can have complicated geometrical configuration and hence significant local pressure losses.

Fig. 13 shows the steady state mass flow rate from various uniform gap widths of an annular loop as a function of the non-dimensional group $Gr_m(2a/L)$. The modified Grashof number Gr_m has been introduced by Vijayan et al. (1991), and is defined using the present symbols:

$$Gr_m = \frac{\rho^2 g\beta(2a)^3\Delta T_r}{\mu^2} \quad \text{with} \quad \Delta T_r = \frac{Q_h \Delta Z}{A\mu c_p} \tag{15}$$

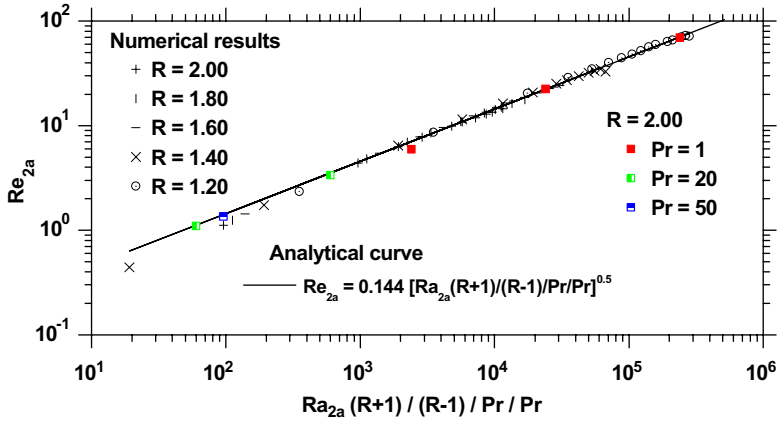

Fig. 13. Evolution of the Reynolds number as a function of the non-dimensional number $Gr_m(2a/L)$ for various radius ratios.

Table 3
Mean and local values for various Prandtl numbers, $R = 2.0$

Pr	Ra	$Gr_m(2a/L)$	$[Ra_{2a}(R-1)/(R+1)]^{0.5}$	$f_F Re_{2a}$	Re_{2a}	Eq. (16)	$\overline{Nu}_c$	$\overline{\Theta}_h$
1	10^2	2400	16.33	22.74	5.92	7.06	9.41	1.76
1	10^3	24 000	51.64	22.37	22.45	22.31	8.61	0.667
1	10^4	240 000	163.3	24.00	69.19	70.55	9.29	0.454
20	10^3	60	51.64	22.37	1.03	1.11	8.62	0.668
20	10^4	600	163.3	23.73	3.38	3.53	9.18	0.462
50	10^4	96	163.3	23.79	1.36	1.41	9.18	0.460
50	2×10^4	192	230.9	24.56	1.52	2.00	9.36	0.448

Q_h is the heater power and A the cross-section area. As recommended by Vijayan (2002), ΔZ, the center line elevation difference between the cooler and the heater is used instead of the loop height.

In the case of a 2D-annular loop, this gives:

$$Gr_m\left(\frac{2a}{L}\right) = \frac{Ra_{2a}}{Pr^2}\frac{R+1}{R-1}$$

Using the theoretical correlation of the friction factor for fully developed forced flow in a plane wall channel for laminar flow, $f_{DW} = \frac{p}{Re_{2a}^b} = \frac{96}{Re_{2a}}$, the proposed correlation of Vijayan (2002) can thus be expressed as

$$Re_{2a} = \left(\frac{2}{p}\right)^{1/(3-b)}\left(Gr_m\frac{2a}{L}\right)^{1/(3-b)} = 0.144\left(\frac{Ra_{2a}}{Pr^2}\frac{R+1}{R-1}\right)^{0.5} \quad (16)$$

The numerical data are adequately represented by the theoretical correlation (Fig. 13) except at very low values, for which small deviations can be seen, the regime being pseudo-conductive. It must be remarked that the numerical friction factor calculated using Eq. (9) gives results which are very closed to the analytical value. Numerically, it is found that $f_F Re_{2a} = 23.15 \pm 0.84$ (over 80 runs, see Table 2 for some particular values) while the analytical value is 24. It can be concluded that the friction factor is neither greatly affected by recirculation nor by curvature effect.

The present numerical experiment corroborates the fact that forced flow correlations are assumed to be applicable for natural circulation flow only if the pressure losses can be neglected, and in laminar regions theoretical correlation Eq. (16) gives good results in establishing the validity of the proposed dimensionless group. In cases where local pressure losses are non-negligible compared with, they should be taken into account as an equivalent extra length L' (Eq. (16)).

Finally, the Reynolds correlation has been validated versus the Prandtl number dependence. To do this, some extra computations have been performed for three different values of the Prandtl number, 1, 20, 50 and for one given radius ratio, $R = 2.0$. All these results are also reported in Table 3. As can be seen in Fig. 13 (square symbols), the accuracy of Eq. (16) is very good, at least for this range of the Prandtl numbers. Moreover, the heat transfer results, the cold mean Nusselt number (Fig. 11) and the mean heat temperature (Fig. 12), show that the dependence on Prandtl number is weak.

4. Conclusions

Natural convection in a 2D-annular closed-loop thermosyphon filled with water has been numerically investigated.

The numerical results showed that local recirculation occurs near the two connections at the outer cylinder, the larger being at the heater entrance owing to its heating imposing heat flux. Compared with natural convection in a toroidal loop, the local flow reversal only prevails near the outer wall in an annular loop.

It has been numerically demonstrated that forced flow correlations are assumed to be applicable for natural circulation flow in a 2D-annular thermosyphon. This is presumably due to the absence of pressure losses due to the presence of bends and flow area changes. In this simple case, the friction factor has been numerically calculated, and is almost unaffected by the recirculation regions.

This also demonstrated the very weak influence of the curvature, the correlation used being that of a plane-wall channel.

The non-dimensional group $[Ra_{2a}(R-1)/(R+1)]^{0.5}$ rather than the Rayleigh number is shown to be more appropriate to the evolution of the average heat transfer data for experimental values (temperatures and Nusselt numbers).

Finally, this paper has also demonstrated, that it is possible to find numerically, by brute force integration of the classical Navier–Stokes equations, transient, oscillatory and reverse flow motions in thermosyphon that have been experimentally found in toroidal loops. These results now need experimental verification in the case of an annular loop.

Acknowledgments

The authors acknowledge the help of R. Spampinato with some of the computational work. The support by the French National Institute for Advances in Scientific Computations (IDRIS-Computer Center) project no. 03 1265 is gratefully acknowledged.

References

Basaran, T., Kucuka, S., 2003. Flow through rectangular thermosyphon at specified wall temperatures. Int. Commun. Heat Mass Transfer 30 (7), 1027–1039.

Bernier, M.A., Baliga, B.R., 1992. A 1D/2D model and experimental results for a closed-loop thermosyphon with vertical heat transfer sections. Int. J. Heat Mass Transfer 35 (11), 2969–2982.

Cadiou, P., 1997. Contribution à l'étude numérique des transferts de chaleur par convection naturelle ou par convection mixte dans une cavité annulaire horizontale. Ph.D. thesis. University of Marne-la-Vallée.

Cadiou, P., Desrayaud, G., Lauriat, G., 1998. Natural convection in a narrow horizontal annulus: the effects of thermal and hydrodynamic instabilities. J. Heat transfer 120, 1019–1026.

Cammarata, G., Desrayaud, G., Fichera, A., Pagano, A., 2002. An ordinary differential model for rectangular natural circulation loops. In: 12th Int. Heat Transfer Conference (Grenoble, France), vol. 2, pp. 273–278.

Creveling, H.F., De Paz, J.F., Baladi, J.Y., Schoenhals, R.J., 1975. Stability characteristics of a single phase free convection loop. J. Fluid Mech. 67 (1), 65–84.

Damerell, P.S., Schoenhals, R.J., 1979. Flow in a toroidal thermosyphon with angular displacement of heated and cooled section. J. Heat Transfer 101, 672–676.

Desrayaud, G., Cadiou, P., Lauriat, G., 2000. Thermoconvective instabilities in a narrow horizontal air-filled annulus. Int. J. Heat Fluid Flow 21 (1), 65–73.

Ehrhard, P., Muller, U., 1990. Dynamical behaviour of natural convection in a single-phase loop. J. Fluid Mech. 217, 487–518.

Gorman, M., Widman, P.J., Robbins, K.A., 1986. Nonlinear dynamics of convection loop: a quantitative comparison of experiment with theory. Physica D 19, 255–267.

Greif, R., 1988. Natural circulation loops. J. Heat transfer 110, 1243–1258.

Huang, B.J., Zelaya, R., 1988. Heat transfer behaviour of a rectangular thermosyphon. J. Heat transfer 110, 487–493.

Jiang, Y.Y., Shoji, M., Naruse, M., 2002. Boundary condition effects on the flow stability in a toroidal thermosyphon. Int. J. Heat Fluid Flow 23, 81–91.

Keller, J., 1966. Periodic oscillations in a model of thermal convection. J. Fluid Mech. 26 (1), 599–606.

Kuehn, T.H., Goldstein, R.J., 1976. An experimental and theoretical study of natural convection in the annulus between horizontal concentric cylinders. J. Fluid Mech. 74 (4), 695–719.

Lavine, S., Greif, R., Humphrey, J.A.C., 1987. A three-dimensional analysis of natural convection in a toroidal loop—the effect of Grashof number. Int. J. Heat Mass Transfer 30, 251–261.

Malkus, W.R.V., 1972. Non-periodic convection at high and low Prandtl number. Mem. Soc. R. Sci. Liege 4kk, 125–128.

Mertol, A., Greif, R., Zvirin, Y., 1982. Two-dimensional study of heat transfer and fluid flow in a natural convection loop. J. Heat Transfer 104, 508–514.

Misale, M., Frogheri, M., Ruffino, P., D'Auria, F., 1998. Steady state and stability behavior of a single-phase natural circulation loop. In: 11th Int. Heat Transfer Conference (Kyongju, Korea), vol. 3, pp. 385–390

Misale, M., Ruffino, P., Frogheri, M., 2000. The influence of the wall thermal capacity and axial conduction over a single-phase natural circulation loop: 2-D numerical study. Heat Mass Transfer 36, 533–539.

Powe, R.E., Carley, C.T., Bishop, E.H., 1969. Free convective flow patterns in cylindrical annuli. J. Heat Transfer 91, 310–314.

Sano, O., 1991. Cellular structure in a natural convection loop and its chaotic behavior. I. Experiment. Fluid Dyn. Res. 8, 189–204.

Stern, C.H., Greif, R., Humphrey, J.A.C., 1988. An experimental study of natural convection in a toroidal loop. J. Heat Transfer 110, 877–884.

Su, Y., Chen, Z., 1995. 2-D numerical study on a rectangular thermosyphon with vertical or horizontal heat transfer sections. Int. J. Heat Mass Transfer 38 (17), 3313–3317.

Vijayan, P.K., 2002. Experimental observations on the general trends of the steady state and stability behaviour of single-phase natural circulation loops. Nucl. Eng. Des. 215, 139–152.

Vijayan, P.K., Austregesilo, H., 1994. Scaling laws for single-phase natural circulation loops. Nucl. Eng. Des. 152, 331–347.

Vijayan, P.K., Mehta, S.K., Date, A.W., 1991. On the steady state performance of natural circulation loops. Int. J. Heat Mass Transfer 34 (9), 2219–2230.

Welander, P., 1967. On the oscillatory instability of a differentially heated fluid loop. J. Fluid Mech. 29 (1), 17–30.

Zvirin, Y., 1981. A review of natural circulation loops in pressurized water reactors and other systems. Nuclear Eng. Des. 67, 203–225.